2008 IEEE International Conference on
Robotics and Automation
Pasadena, CA, USA, May 19-23, 2008

Modeling of Biomimetic Robotic Fish Propelled by an Ionic Polymer-Metal Composite Actuator

Ernest Mbemmo, Zheng Chen, Stephan Shatara, and Xiaobo Tan

Abstract— **In this paper a physics-based model is proposed for a biomimetic robotic fish propelled by an ionic polymer-metal composite (IPMC) actuator. Inspired by biological fins, a passive plastic foil is attached to the IPMC beam. The model incorporates both IPMC actuation dynamics and the hydrodynamics, and captures the interactions between the IPMC actuator and the plastic foil. Experimental results have shown that the proposed model is able to predict the steady-state cruising speed of the robotic fish under a periodic actuation input. Since the majority of the model parameters are expressed in terms of fundamental physical properties and geometric dimensions, the model is expected to be instrumental in optimal design of the robotic fish.**

I. INTRODUCTION

Aquatic animals (e.g., fishes, cetaceans) are ultimate examples of superior swimmers as a result of millions of years of evolution, endowed with a variety of morphological and structural features for moving through water with speed, agility, and efficiency [1]. Intrigued by the remarkable feats in biological swimming and driven by the desire to mimic such capabilities, extensive theoretical, experimental, and computational research has been conducted to understand hydrodynamic propulsion and maneuvering. Recent years have also witnessed significant effort in the development of aquatic robots; see, e.g., [2]–[7]. Most of these robots, however, used motors as actuators to drive rigid foils, which tend to be big, power-hungry, and noisy.

For millimeter to centimeter-size robots, smart material actuators have been explored for propulsion due to their higher energy conversion efficiency and quieter operation compared to traditional motors. A particularly promising class of robotic fish are propelled by ionic polymer-metal composite (IPMC) actuators; see [8], [9], to name a few.

IPMC's form an important category of electroactive polymers (also known as artificial muscles) and have built-in actuation and sensing capabilities [10]. An IPMC sample typically consists of a thin ion-exchange membrane (e.g., Nafion), chemically plated on both surfaces with a noble metal as electrode. When a voltage is applied across an IPMC, transport of hydrated cations and water molecules within the membrane and the associated electrostatic interactions lead to bending motions, and hence the actuation effect.

This research was supported in part by an NSF CAREER grant (ECS 057131) and MSU IRGP (05-IRGP-418)

E. Mbemmo, Z. Chen, S. Shatara and X. Tan are with Department of Electrical & Computer Engineering Michigan State University, East Lansing, MI 48824, USA. mbernest@hotmail.com, chenzhe1@egr.msu.edu, shataras@msu.edu, xbtan@egr.msu.edu

Send correspondence to X. Tan. Tel: 517-432-5671; Fax: 517-353-1980.

Fig. 1 illustrates the mechanism of the IPMC actuation. Because of their softness, resilience, and the capability of producing large deformation under a low action voltage in water, IPMCs are very attractive materials for the applications in biomimetic robots [8], [9], [11].

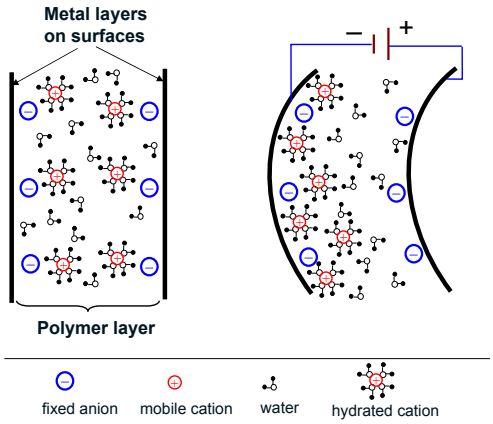

Fig. 1. Illustration of IPMC actuation mechanism (sectional view).

A faithful model for robotic fish propelled by IPMC actuators is desirable for both design and control of the robotic fish. The challenge in the modeling work is that both the hydrodynamics of the robotic fish and the actuation dynamics of IPMC are coupled in a complex manner.

In this paper a physics-based model is proposed for the motion of robotic fish propelled by IPMC actuators. This is achieved by incorporating both the slender-body propulsion theory of Lighthill [12], [13] and the actuation model of IPMCs recently developed by Chen and Tan [14]. The model is capable of predicting the steady-state cruising speed of the robotic fish given a periodic actuation voltage. Inspired by the biological fin structure, we further consider a hybrid fin with a passive plastic piece attached to the IPMC actuator. The proposed model is extended to capture the interactions between the IPMC and the passive fin.

Experiments have been performed to verify the proposed model. It is found that the model can predict well the cruising speed of the robot at different operating frequencies, for different tail dimensions. Experimental results have also confirmed that with a proper passive fin, the fish speed can be significantly improved despite its loading effect on the IPMC actuator. Since most of the parameters in the proposed model are expressed in terms of fundamental physical properties and geometric dimensions, the model will be instrumental for optimal design of the IPMC-propelled robotic fish to achieve high speed and efficiency.

The remainder of the paper is organized as follows. The robotic fish is described in Section II. The proposed model is presented in Section III. Experimental results on model validation are presented in Section IV. Finally, concluding remarks are provided in Section V.

II. IPMC-PROPELLED ROBOTIC FISH

Fig. 2 shows the robotic fish used in this study. It is an upgraded version from that reported in [9]. The fish is designed to be fully autonomous and serve as a mobile, aquatic sensing platform. It consists of a rigid body and an IPMC caudal fin. The IPMC actuator is further covered by a passive plastic fin to enhance propulsion. The rigid shell of the fish was custom-made to reduce the wetted surface while having enough interior room to house rechargeable batteries and various electronic components for control, sensing, wireless communication, and navigation. All these components are contained in a water-proof packaging with necessary wires and pins exposed for charging batteries and driving IPMC actuator. Without the tail, the fish measures 14.8 cm long, 6.3 cm high, and 5.2 cm wide. The tail is about 5 cm long. The total weight of the robotic fish is about 140 g. The shape and configuration of the robot put it into the category of carangiform fish [1].

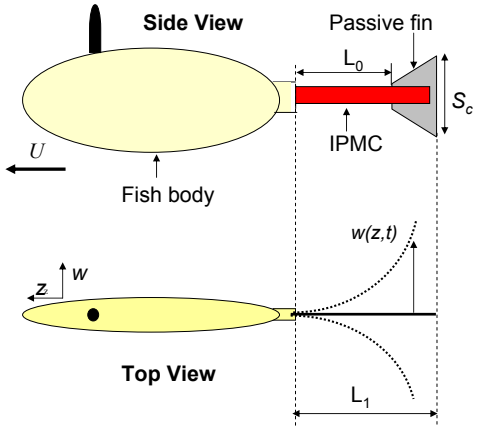

(a)

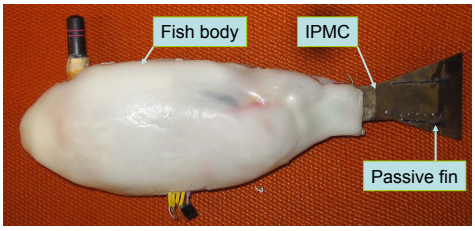

(b)

Fig. 2. (a): Schematic of the robotic fish; (b): Photo of robotic fish.

III. MODELING OF THE ROBOTIC FISH MOTION

The major goal of this paper is to understand the governing dynamics of the IPMC-propelled robotic fish, capture the interactions between the fluid, the fish body, the IPMC actuator, and the passive plastic fin, and thus develop guidelines for optimal design of the robotic fish. In particular, given a periodic voltage input to the IPMC, we want to understand what would be the steady-state cruising speed U of the fish. The model predicting the speed U shall be expressed in terms of fundamental physical parameters and geometric dimensions of various parts (body, IPMC, passive fin) only, so that it is scalable and can be used for design purposes. This is achieved in this paper by merging hydrodynamics with the internal actuation dynamics of IPMC.

A. Lighthill's Theory of Slender-body Propulsion

The starting point of our model is Lighthill's theory of slender-body propulsion [13]. A body is considered slender if its cross-sectional area of the body changes slowly along its length. The robotic fish described in Section II is thus slender and Lighthill's theory applies.

Suppose that the tail is bending periodically with the bending at z denoted by $w(z,t)$. At the steady state, the fish will achieve a periodic, forward motion with some mean speed U. In the discussion here, the word "mean" refers to the average over one period. The mean thrust $\overline{T}$ produced by the tail can be calculated as

$$\overline{T} = \left[\frac{m}{2}\cdot\left(\overline{\left(\frac{\partial w(z,t)}{\partial t}\right)^2} - U^2\cdot\overline{\left(\frac{\partial w(z,t)}{\partial z}\right)^2}\right)\right]_{z=L}, \quad (1)$$

where $z=L$ denotes the end of tail, $\overline{(\cdot)}$ denotes the *mean* value, m is the virtual mass density at $z=L$, expressed as

$$m = \frac{1}{4}\pi S_c^2 \rho_w \beta \ . \quad (2)$$

In (2), S_c is the width of the tail at the end $z=L$, ρ_w is the fluid density, and β is a non-dimensional parameter close to 1. Eq. (1) indicates that the mean thrust depends only on the lateral velocity of the tail $\frac{\partial w}{\partial t}$ and the slope $\frac{\partial w}{\partial z}$ at the tail end.

The cruising fish will experience a drag force F_D:

$$F_D = \frac{C_D\cdot\rho_w\cdot U^2\cdot S}{2}\ , \quad (3)$$

where S is the wetted surface area, and C_D is the drag coefficient. At the steady state, the mean thrust $\overline{T}$ is balanced by the drag F_D, from which one can solve the cruising speed U:

$$U = \left[\sqrt{\frac{m\cdot\overline{\left(\frac{\partial w(z,t)}{\partial t}\right)^2}}{C_D\rho_w S + m\cdot\overline{\left(\frac{\partial w(z,t)}{\partial z}\right)^2}}}\right]_{z=L} . \quad (4)$$

Since the speed of the fish is related to the lateral velocity and the slope at the end of the tail, one needs to fully understand the actuation dynamics of the tail. In the following subsections, we will consider two cases: 1) the tail is an IPMC actuator only; and 2) the tail consists of an IPMC and a passive plastic fin. The latter is inspired by biological fish fins with passive membranes actuated by muscles.

B. Model of Fish Motion with IPMC Tail Only

Chen and Tan recently derived a control-oriented yet physics-based model for IPMC actuators [14]. The model is geometrically scalable and represented in a form of infinite-dimensional transfer function relating the bending displacement $w(z,s)$ of IPMC beam to the voltage input $V(s)$. Here $w(z,s)$ denotes the Laplace transform of the bending motion $w(z,t)$, and s is the Laplace variable. Consider Fig. 3, where the beam is clamped at one end ($z=0$), and the actuation voltage is applied at the same location.

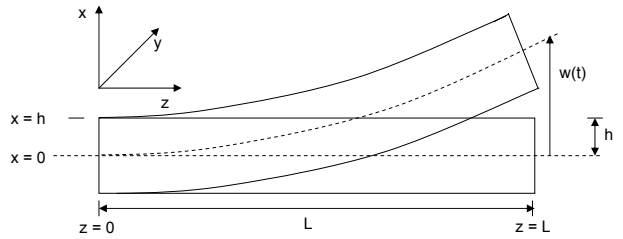

Fig. 3. Geometric definitions of an IPMC beam in the cantilevered configuration (side view).

The transfer function $H_1(z,s)$ relating $w(z,s)$ to $V(s)$ is a product of two modules, $\Gamma(z,s)$ and $G(s)$:

$$H_1(z,s) = \frac{w(z,s)}{V(s)} = \Gamma_1(z,s)\cdot G(s), \tag{5}$$

where $\Gamma_1(z,s)$ captures the bending-moment generation dynamics due to actuation, and $G(s)$ represents the viscoelastic dynamics of the IPMC beam. $\Gamma(z,s)$ is expressed as [14]:

$$\Gamma_1(z,s) = \frac{\alpha_0 W}{Y_e I}\frac{Kk_e(\gamma-1)}{(\gamma s+K)}\left(\frac{X(z,s)}{1+r_2\theta(s)}\right), \tag{6}$$

where α_0 is the stress-charge coupling constant, W is the width of IPMC, κ_e is the effective dielectric constant of the polymer, $I=\frac{2Wh^3}{3}$ is the inertial moment of IPMC beam, and r_2 is the electrode resistance per unit length in x direction. Y_e is the equivalent Young's modulus of IPMC in the fluid [15]:

$$Y_e = \frac{Y}{\left(1+\frac{\pi\rho_w W}{8\rho_c h}\right)},$$

where ρ_c is the density of IPMC, and Y is its Young's modulus (in air). K and γ are constants defined as:

$$K \triangleq \frac{F^2 dC^-}{\kappa_e RT}\left(1-C^-\Delta V\right),\ \gamma=\sqrt{\frac{K}{d}}h\ ,$$

where F is Faraday's constant, d is the ionic diffusitivity, C^- is the anion concentration in IPMC, R is the gas constant, T is the absolute temperature, and ΔV is the volumetric change. The other functions in (6) are defined as:

$$\theta(s) = \frac{Wk_e s\gamma(s+K)}{h(s\gamma+K)}\ ,\ B(s)=\sqrt{r_1\left(\frac{\theta(s)}{(1+r_2\theta(s))}+\frac{2}{R_p}\right)}\ ,$$

$$X(z,s) = \frac{1+(\sinh(B(s)z)-B(s)z)\tanh(B(s)L)-\cosh(B(s)z)}{B(s)^2}\ ,$$

where r_1 is the electrode resistance per unit length in z direction and R_p is the through-polymer resistance per unit length.

The viscoelastic dynamics $G(s)$, due to the relative low actuation bandwidth of IPMC, can be described by a second-order system:

$$G(s) = \frac{\omega_n^2}{s^2+2\xi\omega_n+\omega_n^2}\ , \tag{7}$$

where ω_n is the natural frequency of the IPMC cantilever beam in fluid, and ξ is the damping ratio. Since the Reynolds number Re of the IPMC beam in water satisfies $Re >> 1$, the inviscid fluid model is applicable. The natural frequency ω_n can be expressed in terms of the beam dimensions and mechanical properties [15]:

$$\omega_n = \frac{C_1^2}{L^2}\sqrt{\frac{Y_e I}{2\rho_c W h}}\ , \tag{8}$$

where C_1 is the constant associated with the first-mode oscillation.

To couple the actuation dynamics to hydrodynamics, we derive the transfer function $H_{1d}(z,s)$ relating the slope of the beam $\frac{\partial w(z,s)}{\partial z}$ to the input voltage $V(s)$,

$$H_{1d}(z,s) = \frac{\frac{\partial w(z,s)}{\partial z}}{V(s)} = \Gamma_{1d}(z,s)\cdot G(s), \tag{9}$$

$$\Gamma_{1d}(z,s) = \frac{\psi_s W}{Y_e I}\frac{Kk_e(\gamma-1)}{(\gamma s+K)} \cdot\frac{(\cosh(B(s)z)-1)\tanh(B(s)L)-\sinh(B(s)z)}{B(s)(1+r_2\theta(s))}\ .$$

Given the input voltage $V(t)=A_m\sin(\omega t)$, the bending displacement and the slope of the IPMC at the end can be written by,

$$w(L,t) = A_m|H_1(L,j\omega)|\sin(\omega t+\angle H_1(L,j\omega)), \tag{10}$$

$$\frac{\partial w(L,t)}{\partial z} = A_m|H_{1d}(L,j\omega)|\sin(\omega t+\angle H_{1d}(L,j\omega)), \tag{11}$$

where $\angle(\cdot)$ denotes the phase angle.

From (4), (10), and (11), one can obtain the fish speed U under the actuation voltage $V(t)=A_m\sin(\omega t)$ by

$$U = \sqrt{\frac{mA_m^2\omega^2|H_1(L,j\omega)|^2}{2C_D\rho_w S+mA_m^2|H_{1d}(L,j\omega)|^2}}\ . \tag{12}$$

C. Model of Fish Motion With Hybrid Tail

From (1) and (2), the tail width S_c at the end has a significant impact on the speed U. One could increase S_c by simply using a wider IPMC beam. Due to IPMC mechanism, however, a too wide beam (i.e., plate) will produce cupping instead of bending motion and is thus not desirable. Therefore, it has been chosen to increase the edge width by attaching a passive plastic piece, as illustrated in Fig. 4. Although such a hybrid tail is expected to increase the thrust, one has to also consider that the extra hydrodynamic force on the passive fin adds to the load of IPMC and may reduce

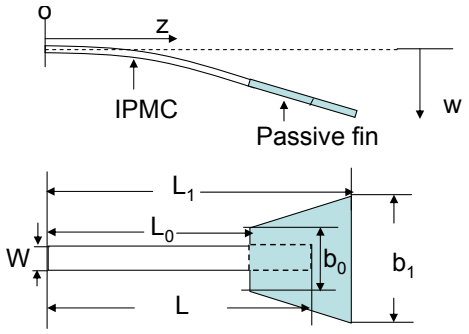

Fig. 4. IPMC beam with a passive fin.

the bending amplitude. Therefore, it is necessary to model these interactions carefully.

The hydrodynamic force acting on the passive fin can be written as [15]

$$F_{hydro}(z,s) = -\frac{\pi}{4}\rho_w s^2 b(z)^2 \Gamma(s) w(z,s) \ , \qquad (13)$$

where $L_0 \le z \le L_1$ and $\Gamma(s) \approx 1$ for inviscid water. Eq. (13) essentially says that the hydrodynamic force equals the virtual mass multiplied by the acceleration. Note that the hydrodynamic force acting on the active IPMC beam has been incorporated in the derivation of the equivalent Young's modulus of the IPMC in fluid [15], so only the hydrodynamic force on the passive fin needs to be considered here. Since the passive fin is rigid compared to IPMC, its width $b(z)$ and deflection $w(z,s)$, $L_0 \le z \le L_1$, can be written as

$$\begin{aligned} b(z) &= \frac{b_1 - b_0}{L_1 - L_0}(z - L_0) + b_0 \ , \\ w(z,s) &= w(L_0,s) + \frac{\partial w(L_0,s)}{\partial z}(z - L_0) \ , \end{aligned} \qquad (14)$$

where b_0, b_1, L, L_0, L_1 are as defined in Fig. 4. For any point z on the IPMC beam, $z \le L_0$, the bending moment generated by the hydrodynamic force acting on the passive fin is

$$M_{tail}(z,s) = \int_{L_0}^{L_1} F_{hydro}(\tau,s)(\tau - z)\, d\tau \ . \qquad (15)$$

The deformation $w(z,s)$ of the IPMC is governed by

$$\frac{\partial^2 w(z,s)}{\partial z^2} = \frac{M_{IPMC}(z,s) - M_{tail}(z,s)}{Y_e I} \ , \qquad (16)$$

where $0 \le z \le L_0$ and M_{IPMC} is the moment generated by the IPMC actuation process. The bending displacement along the IPMC beam is then

$$w(z,s) = \int_0^z \int_0^\tau \frac{M_{IPMC}(v,s) - M_{tail}(v,s)}{Y_e I} dv d\tau \ . \qquad (17)$$

From the actuation model of IPMC, (5),

$$\int_0^z \int_0^\tau \frac{M_{IPMC}(v,s)}{Y_e I} dv d\tau = \Gamma_1(z,s) V(s) \ . \qquad (18)$$

Integrating (17), the transfer functions relating $w(L_0,s)$ and $w'(L_0,s) \triangleq \frac{\partial w(L_0,s)}{\partial z}$ to $V(s)$ can be found:

$$H_2(L_0,s) = \frac{w(L_0,s)}{V(s)} = \Gamma_2(L_0,s)\cdot G(s) \qquad (19)$$

$$H_{2d}(L_0,s) = \frac{w'(L_0,s)}{V(s)} = \Gamma_{2d}(L_0,s)\cdot G(s) \ , \qquad (20)$$

$$\begin{aligned} \Gamma_2(L_0,s) &= \frac{(1-F)A + BE}{(1-C)(1-F) - BJ} \ , \\ \Gamma_{2d}(L_0,s) &= \frac{(1-C)E + AJ}{(1-C)(1-F) - BJ} \ , \end{aligned} \qquad (21)$$

$$A = \Gamma_1(L_0,s) \ , \quad E = \Gamma_{1d}(L_0,s) \ , \ D = L_1 - L_0 \ , \ k = \frac{b_1 - b_0}{D},$$

$$\begin{aligned} B &= \frac{\pi}{4}\frac{s^2\rho_w}{Y_e I}\left[\begin{array}{l} \frac{k^2D^5}{10} + \frac{kb_0}{4}D^4 + \frac{b_0^2}{6}D^3 \\ + \frac{k^2D^4L_0}{12} + \frac{2kb_0D^3L_0}{9} + \frac{b_0^2D^2L_0}{6} \end{array} \right] L_0^2 \ , \\ C &= \frac{\pi}{4}\frac{s^2\rho_w}{Y_e I}\left[\begin{array}{l} \frac{k^2D^4}{8} + \frac{kb_0D^3}{3} + \frac{b_0^2D^2}{4} \\ + \frac{k^2D^3L_0}{9} + \frac{kb_0D^2L_0}{3} + \frac{b_0^2DL_0}{3} \end{array} \right] L_0^2 \ , \\ F &= \frac{\pi}{4}\frac{s^2\rho_w}{Y_e I}\left[\begin{array}{l} \frac{k^2D^5}{5} + \frac{(2kb_0)}{4}D^4 + \frac{\left(b_0^2\right)}{3}D^3 \\ + \frac{k^2D^4L_0}{8} + \frac{kb_0D^3L_0}{3} + \frac{b_0^2D^2L_0}{4} \end{array} \right] L_0 \ , \\ J &= \frac{\pi}{4}\frac{s^2\rho_w}{Y_e I}\left[\begin{array}{l} \frac{k^2D^4}{4} + \frac{2kb_0D^3}{3} + \frac{b_0^2D^2}{2} \\ + \frac{k^2D^3L_0}{6} + \frac{kb_0D^2L_0}{2} + \frac{b_0^2DL_0}{2} \end{array} \right] L_0 \ . \end{aligned}$$

From (14), (19) and (20), one can obtain the transfer functions relating the bending displacement and the slope at $z = L_1$ to the voltage input $V(s)$ as follows:

$$\begin{aligned} H_3(L_1,s) &= \frac{w(L_1,s)}{V(s)} = H_2(L_0,s) + H_{2d}(L_0,s)D \\ H_{3d}(L_1,s) &= \frac{w'(L_1,s)}{V(s)} = H_{2d}(L_0,s). \end{aligned} \qquad (22)$$

Given the input voltage $V(t) = A_m \sin(\omega t)$, from(4) and (22), one can find U by

$$U = \sqrt{\frac{mA_m^2\omega^2 |H_3(L_1, j\omega)|^2}{2C_D\rho_w S + mA_m^2 |H_{3d}(L_1, j\omega)|^2}} \ . \qquad (23)$$

IV. EXPERIMENTAL VERIFICATION

A. Experimental Setup

Three different types of experiments have been carried out for model identification and validation: 1) identification of parameters related to the fish body; 2) identification and validation of the IPMC actuation model; 3) validation of the model for fish motion with different tail dimensions.

The most important parameter related to the fish body is the drag coefficient C_D, which depends on the Reynolds number, the fitness ratio of the body, and the properties of the fish surface and fluid. In order to identify C_D, the fish was pulled with different velocities, and metric spring scales were used to measure the drag force F_D. With the measured drag force, velocity, and surface area of the fish, the drag

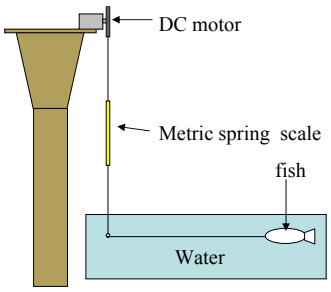

Fig. 5. Illustration of the drag force measurement setup.

coefficient C_D was calculated from (3). Fig. 5 illustrates the experimental setup for drag force measurement.

To investigate the hydrodynamic effect of the plastic fin on IPMC, the frequency responses of the tail subject to voltage input was measured for both without and with the plastic piece. They were also used to verify the actuation model of IPMC, $H_1(L,s)$ and $H_2(L,s)$. Fig. 6 shows the picture of experimental setup. The robotic fish was fixed in the water by a frame arm and a sequence of sinusoidal voltages with amplitude 1.65 V and frequency ranging from 0.05 Hz to 10 Hz were applied to the IPMC. The lateral displacement of the IPMC beam was captured by a laser sensor.

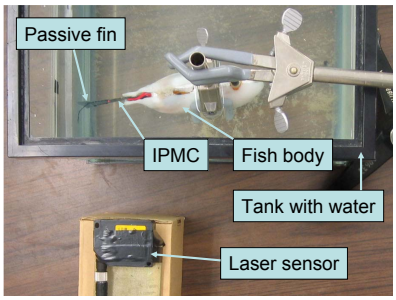

Fig. 6. The experimental setup for identification and verification of IPMC actuation model (top view).

To validate the motion model of the robotic fish, the velocities of the fish propelled by IPMC under different actuation frequencies with amplitude $A_m = 3.3V$ were measured. In this experiment, the robotic fish swam freely in a tank marked with start and finish lines, and a timer recorded the time it took for the fish to travel the designated range. Fig. 7 shows a snapshot of fish swimming in the tank, where one can clearly see the (reverse) Kármán vortex street behind the fish. An accompanying video is attached to this paper.

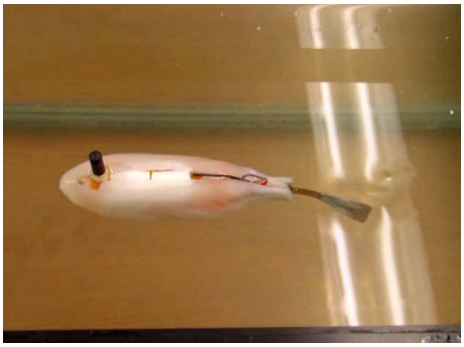

Fig. 7. Snapshot of robotic fish in swimming test.

B. Parameter Identification

Table I shows the identified parameters in the model. The parameters related to the fish body were obtained as discussed in Section IV-A, and the parameters related to IPMC were identified as in [14]. Since $|C^-\Delta V| \ll 1$ [16], we take $1 - C^-\Delta V = 1$.

TABLE I

IDENTIFIED MODEL PARAMETERS.

F	R	T	R_p
96487 C/mol	8.3143 J/mol · K	300 K	34 Ω·m
Y [14]	h	r_1	r_2
5.71×10^8 Pa	175 (μm)	2129 Ω/m	8.2^{-3} Ω· m
d	C^-	κ_e	α_0
3.38×10^{-7} m^2/s	1091 mol/m^3	1.48×10^{-6} F/m	0.05 1/C
C_1	ρ_w	ξ	ρ_c
1.8751	1000kg/m^3	0.225	1600kg/m^3
S	C_D		
1.52×10^{-2}m^2	0.017		

C. Model Validation

The model validation has three parts. First, the actuation model of IPMC with and without passive fin is verified. As shown in Fig. 8 and Fig. 9, good agreement has been achieved between the model prediction (simulation) and the experimental measurement for both cases. Second, the effectiveness of adding a passive fin has been confirmed. As shown in Fig. 10, over 100% improvement in speed can be achieved by adding the passive fin. The dimensions of the fins can be found in Table II. Third, the capability of the model in predicting cruising speed is verified for different operating frequencies, for different tail dimensions. Fig. 11 and Fig. 12 show that for two different fish, Fish A and Fish B (see Table II) with passive fins, the predicted speed matches well the experimental data. This also confirms that the proposed model is scalable and can be used for optimal design and control of the robotic fish.

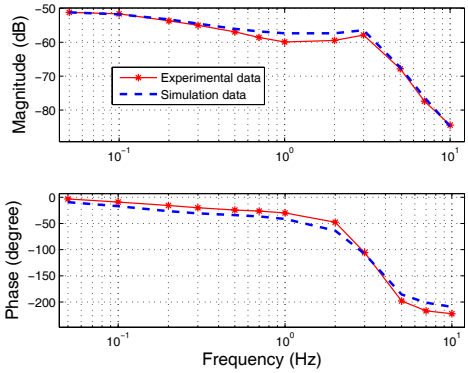

Fig. 8. Validation of IPMC actuation model without a passive fin.

TABLE II

DIMENSIONS OF TWO FISH TAILS.

	L_0(mm)	L_1(mm)	W(mm)	b_0(mm)	b_1(mm)
Fish A	10	51.7	14.7	13	40.5
Fish B	14	34	11	11	30

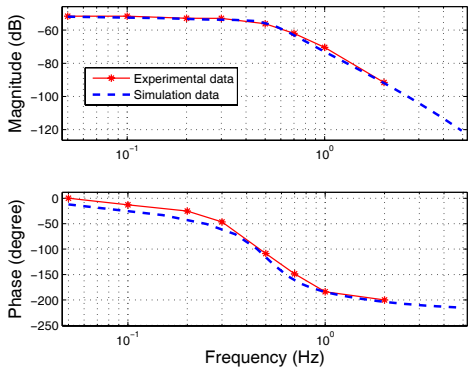

Fig. 9. Validation of IPMC actuation model with a passive fin.

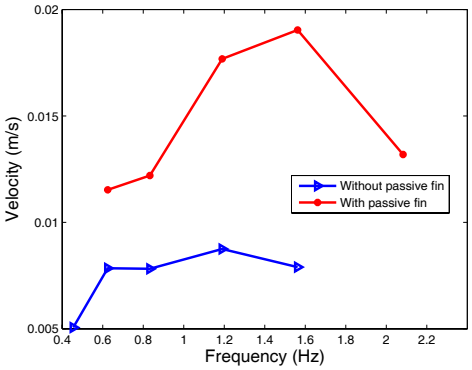

Fig. 10. Measured speed for fish B with and without passive fin.

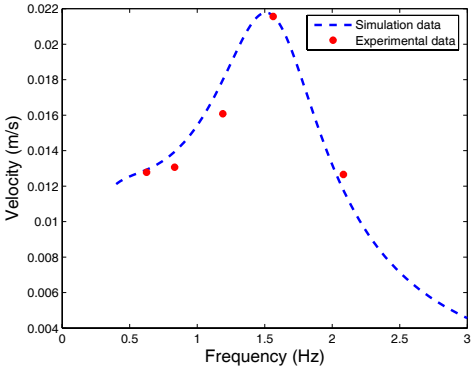

Fig. 11. Verification of motion model for fish A.

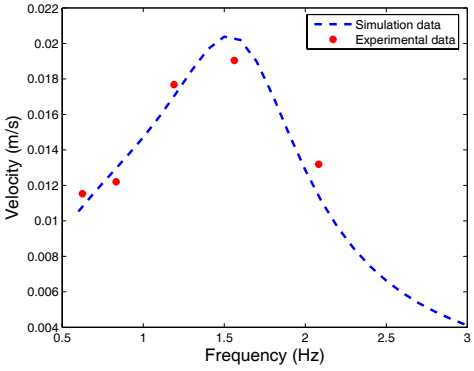

Fig. 12. Verification of motion model for fish B.

V. CONCLUSIONS AND FUTURE WORK

In this paper, the modeling of steady-state cruising motion was presented for an IPMC-propelled robotic fish. The model incorporates both hydrodynamics and IPMC actuation dynamics, and it further considers the hydrodynamic effect of a passive plastic fin. The model was verified in experiments for robotic fish with different tail dimensions. The model is geometrically scalable since most of its parameters can be expressed in terms of fundamental properties of IPMC materials or the fish body. Thus it will be useful for design and control of the robot for improving the cruising speed.

Future work involves extending the model for capturing turning motions and examining optimal turning strategies. Unsteady hydrodynamics of the robotic fish will also be investigated in the interest of fast maneuvering.

REFERENCES

[1] M. Sfakiotakis, D. M. Lane, and J. B. C. Davies, "Review of fish swimming modes for aquatic locomotion," *IEEE Journal of Oceanic Engineering*, vol. 24, no. 2, pp. 237–252, 1999.

[2] M. S. Triantafyllou and G. S. Triantafyllou, "An efficient swimming machine," *Scientific American*, vol. 272, p. 64, 1995.

[3] J. Yu and L. Wang, "Parameter optimization of simplified propulsive model for biomimetic robot fish," in *Proceedings of the 2005 IEEE International Conference on Robotics and Automation*, Barcelona, Spain, 2005, pp. 3306–3311.

[4] J. Liu, I. Dukes, and H. Hu, "Novel mechatronics design for a robotic fish," in *IEEE/RSJ International Conference on Intelligent and Systems*, 2005, pp. 2077–2082.

[5] S. D. Kelly and H. Xiong, "Controlled hydrodynamic interactions in schooling aquatic locomotion," in *Proceedings of the 44th IEEE Conference on Decision and Control, and the European Control Conference 2005*, Seville, Spain, 2005, pp. 3904–3910.

[6] P. Kodati and X. Deng, "Experimental studies on the hydrodynamics of a robotic ostraciiform tail fin," in *Proceedings of the 2006 IEEE/RSJ International Conference on Intelligent Robots and Systems*, Beijing, China, 2006, pp. 5418–5423.

[7] K. A. Morgansen, B. I. Triplett, and D. J. Klein, "Geometric methods for modeling and control of free-swimming fin-actuated underwater vehicles," *IEEE Transactions on Robotics*, vol. 23, no. 6, pp. 1184–1199, 2007.

[8] S. Guo, T. Fukuda, and K. Asaka, "A new type of fish-like underwater microrobot," *IEEE/ASME Transactions on Mechatronics*, vol. 8, no. 1, pp. 136–141, 2003.

[9] X. Tan, D. Kim, N. Usher, D. Laboy, J.Jackson, A.Kapetanovic, J. Rapai, B. Sabadus, and X. Zhou, "An autonomous robotic fish for mobile sensing," in *Proceedings of the IEEE/RSJ International Conference on Intelligent Robots and Systems*, Beijing, China, 2006, pp. 5424–5429.

[10] M. Shahinpoor and K. Kim, "Ionic polymer-metal composites: I. Fundamentals," *Smart Materials and Structures*, vol. 10, pp. 819–833, 2001.

[11] B. Kim, D. Kim, J. Jung, and J. Park, "A biomimetic undulatory tadpole robot using ionic polymer-metal composite actuators," *Smart Materials and Structures*, vol. 14, pp. 1579–1585, 2005.

[12] M. J. Lighthill, "Note on the swimming of slender fish," *Journal of Fluid Mechanics*, vol. 9, pp. 305–317, 1960.

[13] ——, "Aquatic animal propulsion of high hydromechanical efficiency," *Journal of Fluid Mechanics*, vol. 44, pp. 265–301, 1970.

[14] Z. Chen and X. Tan, "A control-oriented, physics-based model for ionic polymer-metal composite actuators," in *Proceedings of the 46th IEEE Conference on Decision and Control*, New Orleans, LA, 2007, pp. 590–595.

[15] J. E. Sader, "Frequency response of cantilever beams immersed in viscous fluids with applications to the atomic force micrscope," *Journal of Applied Physics*, vol. 84, no. 1, pp. 64–76, 1998.

[16] S. Nemat-Nasser and J. Li, "Electromechanical response of ionic polymer-metal composites," *Journal of Applied Physics*, vol. 87, no. 7, pp. 3321–3331, 2000.